Microfluid Nanofluid (2012) 12:75–84
DOI 10.1007/s10404-011-0850-1

RESEARCH PAPER

Pneumatic dispensing of nano- to picoliter droplets of liquid metal with the StarJet method for rapid prototyping of metal microstructures

A. Tropmann · N. Lass · N. Paust · T. Metz · C. Ziegler · R. Zengerle · P. Koltay

Received: 11 April 2011 / Accepted: 12 July 2011 / Published online: 28 July 2011

Abstract This study presents a new, simple and robust, pneumatically actuated method for the generation of liquid metal micro droplets in the nano- to picoliter range. The so-called StarJet dispenser utilizes a star-shaped nozzle geometry that stabilizes liquid plugs in its center by means of capillary forces. Single droplets of the liquid metal can be pneumatically generated by the interaction of the sheathing gas flow in the outer grooves of the nozzle and the liquid metal. For experimental validation, a print head was build consisting of silicon chips with a star-shaped nozzle geometry and a heated actuator (up to 280°C). The silicon chips are fabricated by Deep Reactive Ion Etching (DRIE). Chip designs with different star-shaped geometries were able to generate droplets with diameters in the range of the corresponding nozzle diameters. The StarJet can be operated in two modes: Either continuous droplet dispensing mode or drop on demand (DoD) mode. The continuous droplet generation mode for a nozzle with 183 µm diameter shows tear-off frequencies between 25 and 120 Hz, while droplet diameters remain constant at 210 µm for each pressure level. Metal columns were printed with a thickness of 0.5–1.0 mm and 30 mm height (aspect ratio >30), to demonstrate the directional stability of droplet ejection and its potential as a suitable tool for direct prototyping of the metal microstructures.

Keywords Rapid prototyping · Metal droplets · Metal printing · Drop on demand · Micro droplets

A. Tropmann (✉) · N. Lass · T. Metz · C. Ziegler · R. Zengerle (✉) · P. Koltay
Department of Microsystems Engineering—IMTEK, University of Freiburg, Georges-Koehler-Allee 106, 79110 Freiburg, Germany
e-mail: artur.tropmann@imtek.uni-freiburg.de

R. Zengerle
e-mail: roland.zengerle@imtek.uni-freiburg.de

N. Paust · R. Zengerle
BIOSS Centre for Biological Signalling Studies, University of Freiburg, Freiburg, Germany

R. Zengerle
Hahn-Schickard-Gesellschaft for Applied Research, Wilhelm-Schickard-Strasse 10, 78052 Villingen-Schwenningen, Germany

P. Koltay
BioFluidix GmbH, Georges-Koehler-Allee 106, 79110 Freiburg, Germany

1 Introduction

The development of rapid prototyping (RP) methods for metallic devices resulted in several different technologies, such as, Selective Laser Sintering (Agarwala et al. 1995), especially Direct Metal Laser Sintering (Wang et al. 2003), Fused Deposition of Metals (Wu et al. 2001), 3D printing (Sachs et al. 1993), stereo lithography techniques (Yamaguchi et al. 1995), and Electron Beam Melting (Larson 1998). Another prominent approach that focuses on the RP of metal microstructures is non-contact printing.

The non-contact printing of liquid droplets in the nano- and picoliter range has become an important field within many scientific communities as well as in industry. Especially, the Micro-Electro-Mechanical Systems (MEMS) technologies have contributed and benefited from non-contact printing in the past 20 years. On one hand, numerous droplet generators have been realized by MEMS technology (Madou 2002), the most prominent being the various types of inkjet print heads (Heinzl and Hertz 1985). On the other hand, there are many applications that require the use of micro droplets, e.g., microarrays printing (De

Heij et al. 2004), or for RP (Essien et al. 2000). A particularly challenging area of non-contact printing is the dispensing of liquid metals (Wehl et al. 2003). Typical applications are the generation of solder bumps (Schuhmacher et al. 2007) for flip chip bonding, RP of electric circuits (Essien et al. 2000), and especially for the RP of metallic devices (Cao and Miyamoto 2006).

Researchers have presented techniques for direct printing of metal, based on various droplet ejection techniques. Hayes et al. (1999) developed an application for micro dispensing and printing of solder using the Ink-Jet technology. Wehl et al. (2006) introduced an extension of their Ink-Jet based dispenser for droplet ejection by an acoustically driven droplet generation. Irlinger and Harnisch (2005) used a heated tube with an integrated ferritic piston, which is electromagnetically displaced. Another droplet generation principle developed by Orme et al. (1993) takes advantage of the capillary stream breakup of a solder jet, that is excited by a piezoelectric actuator to produce solder droplets. Tsung Pan et al. (1998) presented a dispenser which forces droplets out of a nozzle using the effect of the Lorentz force. The groups of Poulikakos (Waldvogel et al. 1996; Haferl et al. 2000; Attinger et al. 2000) and Megaridis et al. (2004), investigated the transport phenomena of micro droplets during droplet deposition on substrates and during the stacking of single drops upon each other (Haferl and Poulikakos 2002). The study of these authors, concentrates rather on the investigation of impact and solidification processes, than on the drop formation in liquid solder jets. As our study does not deal with impact and solidification phenomena of micro drops on substrates, we want to mention the research of the Poulikakos group due to the high relevance of their study in the field of RP with direct deposition of molten metal drops.

The contact free dispensing of liquid metals is desirable in most prototyping applications, but it is also particularly challenging. The droplet generator must operate above the typically high melting temperatures of the metal. The high temperatures and the temperature variation during heating and cooling, can induce mechanical stress that complicates assembly of the devices and boosts oxidation. Preventing oxidation of the jetted droplet is an additional issue. Therefore, in most of the cases, a constant flow of inert gas around the liquid metal is required. If the droplet generators are driven by piezoelectric ceramics (Wehl et al. 2003), the piezoelectric actuators must be thermally insulated as their working range is limited by the Curie temperature that normally ranges between 150 and 300°C. Generally, the thermal insulation of the piezoelectric ceramics has to be done for metals, except for metals with low melting points, such as tin–lead alloys (Sedlacek 1986). Finally, the high surface tension of liquid metals and the very high contact angle on most materials prevent the capillary priming of the dispensing devices.

The StarJet method presented in this study provides a simple solution for the dosage of liquid metals, and does not suffer from any of these issues. It takes advantage of the high contact angle between the liquid metal and the nozzle material, which thereby, enables the working principle described later in more detail. The nozzle is designed in such a manner that, the capillary two-phase flow, involving the liquid metal and a sheath gas, induces a self-regulated and periodical droplet break-off within the nozzle. Nozzle manufacturing requires a specific MEMS dry-etching technique known as Deep Reactive Ion Etching (DRIE), which delivers accurate geometries for the microfluidic features inside the nozzle. The assembly of the nozzle chip into the actuator is kept simple, so that the thermal stresses do not affect the system.

Though the StarJet working principle by itself is fairly simple and does not involve any moving parts, the design and fabrication of the StarJet metal droplet generator and its use for micro RP as presented here, are a highly interdisciplinary and complex endeavor. First of all, the complex fluid dynamics of the two-phase flow inside the nozzle, dominated by capillary forces and geometrical surface effects, which is not fully theoretically described yet, provides an interesting field for fluid dynamics research, and computational fluid dynamics modeling. Furthermore, the fabrication of the star-shaped nozzle chip involves MEMS fabrication technologies, and the associated research to create high definition and high aspect ratio micro structures in silicon. It turns out that, the high contact angle ($\Theta = 156° \pm 3°$) between the metal to be printed and the silicon is favorable for the requirements of the StarJet method. However, in the general case, when other material combinations are to be used, the grafting of the nozzle surface by appropriate surface chemistry to achieve the required high contact angles can become a challenging field of research and technology. Finally, the application of a metal droplet generator to produce micro structures or composite materials by RP, is of highest relevance for researchers in the field of process development, micro engineering, as well as material science.

2 Working principle

2.1 Working principle of the star-shaped nozzle

The StarJet dispensing system mainly consists of two basic parts (Figs. 1, 2). The first part is the actuator providing the liquid reservoir, temperature control, and a pneumatic connection. The second and the most crucial part is the star-shaped silicon nozzle including the microfluidic channels. Besides the two mentioned parts, the experimental setup is formed by the periphery, which consists of

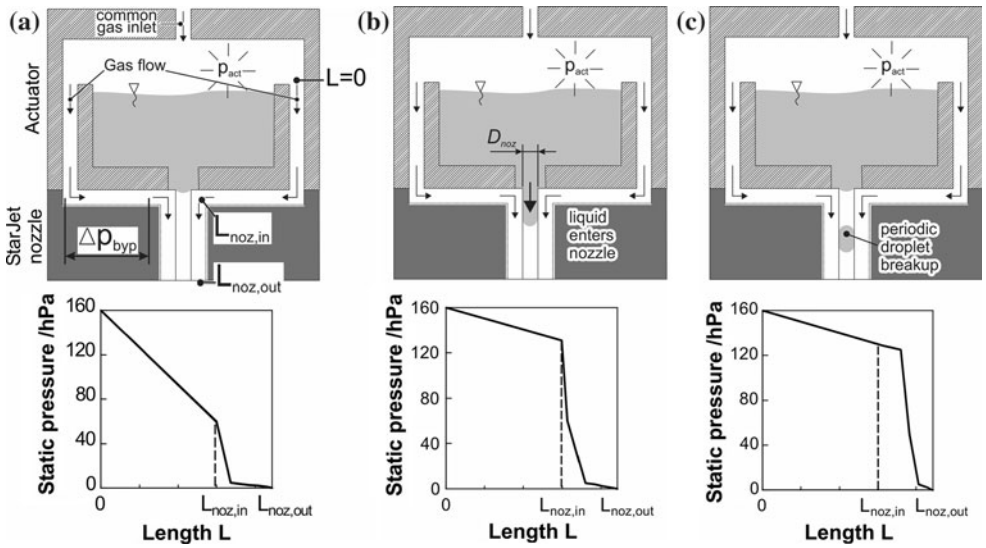

Fig. 1 Schematic sketch of the droplet break-off inside the StarJet dispenser. The magnitude of the actuation pressure (160 hPa) is constant during all the three stages of the droplet break-off. The diagrams depict the calculated static pressures by a CFD simulation as detailed later on. **a** After applying the gas pressure on top of the reservoir, the gas begins to flow around the reservoir leading to a static pressure of 60 hPa at $L_{noz,in}$. **b** When the liquid enters the nozzle, the static pressure increases to 130 hPa at $L_{noz,in}$ and induces the constriction of the liquid column near $L_{noz,in}$. The shear flow of the gas supports the separation of the droplet from the liquid column. **c** The separated droplet is pulled toward the nozzle outlet by the shear flow of the gas. As long as the droplet is not ejected from the nozzle, the pressure at $L_{noz,in}$ is increased and the capillary pressure is larger than the pressure difference Δp_{byp} between the p_{act} and $L_{noz,in}$. Thus, no further liquid can enter the nozzle until the droplet is fully ejected

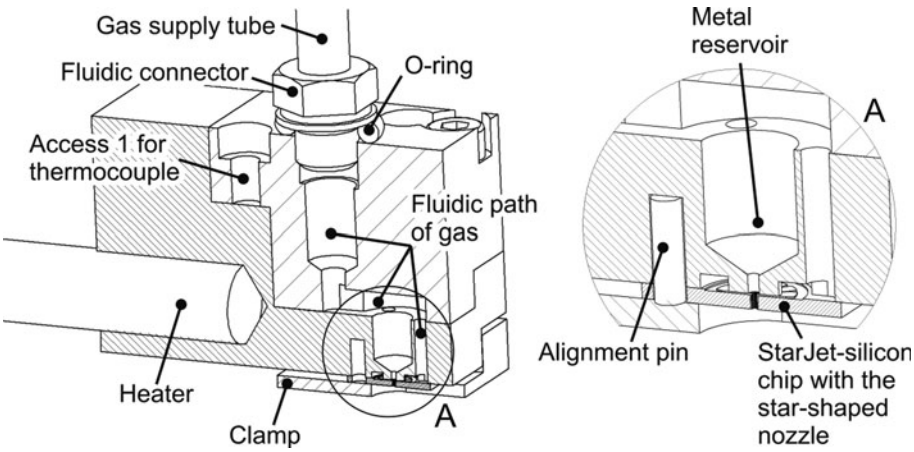

Fig. 2 Design of the actuator used to heat and to establish fluidic connections to the nozzle chip

pneumatic and thermal control elements. These are described in detail in the experimental section at the end of this article. Before presenting the results in detail, the working principle of the StarJet dispenser is described, which is based firstly on the centering of liquids inside a star-shaped nozzle, and secondly, on the propagation, elongation, and the break-off of the liquid column within the nozzle.

One fundamental property of a star-shaped micro nozzle as depicted in Fig. 3 is that, a droplet is centered in the middle of the nozzle if the repellent capillary pressure of the nozzle grooves is too high for the liquid to move into the grooves (ESI-Group 2006; Metz et al. 2009). This effect depends on the critical number N of the nozzle grooves, and the contact angle Θ between the nozzle material and the liquid that is being supplied. The corresponding equation of condition, see Eq. 1, is illustrated in Fig. 4. The graph in Fig. 4 divides the diagram in two regions: The region of the centered liquid columns in the upper part and the region where the liquid fills out the whole channel cross section in the lower part of the diagram. The region above the line depicts the condition, which is required to operate the Start Jet dispenser as described in the following. For example, one would need at least $N = 13$ nozzle grooves or more, to assure the centering of a droplet of a liquid that forms a contact angle of 120° toward the nozzle material. In the case

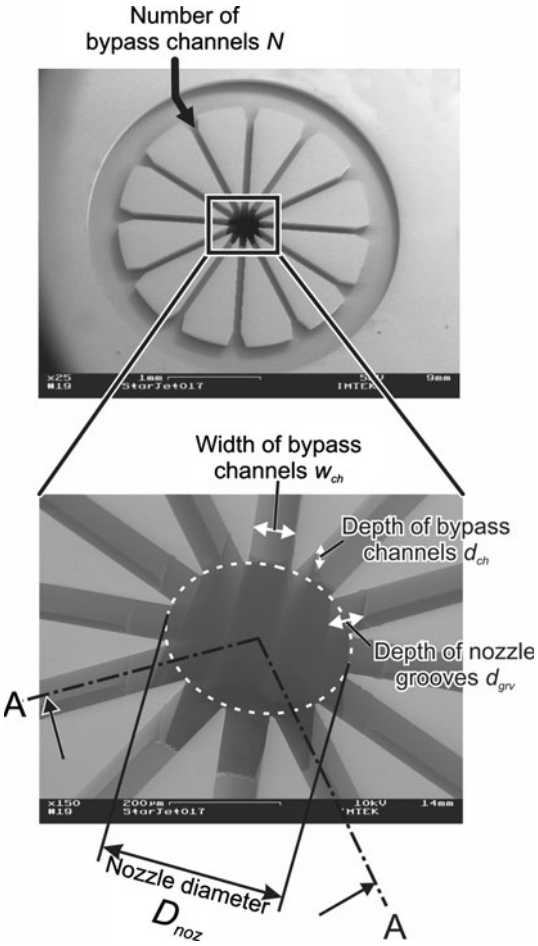

Fig. 3 SEM pictures from the top view of the star-shaped nozzle with corresponding geometrical parameters. The cut *A–A* refers to the sketch in Fig. 5h

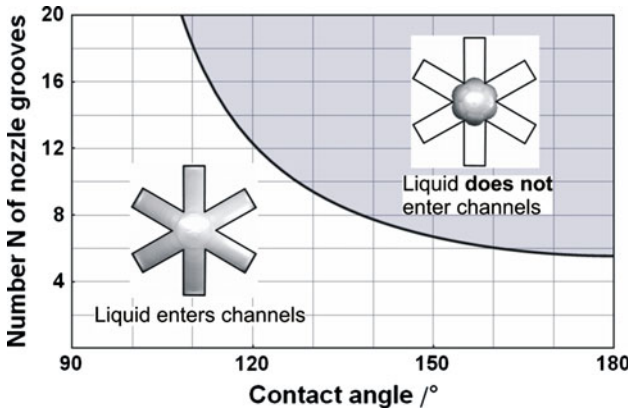

Fig. 4 Number of nozzle grooves (fingers) required for centered droplets as function of the contact angle

of the solder used in this study, which has a contact angle of greater than 150° toward silicon (see Sect. 7 for details), at least seven nozzle grooves are needed. Therefore, only nozzle designs with eight or more grooves are considered in this study. Further details of the capillary mechanism inside the nozzle and a derivation of Eq. 1 are discussed by Metz et al. (2008).

$$N > \pi \cdot \left(\arctan\left(\frac{2\cos^2 \Theta}{2\Theta - \pi - \sin 2\Theta} \right) \right)^{-1} \tag{1}$$

2.2 Droplet break-off mechanism

The disintegration of free flying jets into droplets is typically referred to as Rayleigh–Savart break-up (Rayleigh 1878), caused by an instability and a subsequent minimization of surface energy. A prerequisite for such droplet break-up is that, the droplet diameter is larger than the jet diameter resulting in droplets with smaller surface energy than the jet.

During droplet break-off inside the star-shaped nozzle as observed in experiments, the droplet size is restricted to the jet diameter by the nozzle fingers. The droplets, thus yield higher volume specific surface energy than the liquid column. Consequently, additional energy must be transferred to the liquid to generate the droplets, and a break-off solely driven by a minimization of the surface energy is not possible. In the following, the StarJet break-off mechanism is explained on the basis of a pressure model.

The droplet generation mechanism inside the star-shaped nozzle is illustrated in Fig. 1. The liquid reservoir is placed directly above the inlet of the nozzle chip, which causes a fluidic contact between the liquid reservoir and the gas-carrying bypass channels as shown in Fig. 1a. When applying a pressure to the common inlet, a pressure on the liquid reservoir is established, as well as a gas flow through the bypass channels is induced. This gas flow results in a pressure drop Δp_{byp} along the bypass channels. Since there is a common inlet, the pressure is also applied on the liquid metal surface, and forces a liquid plug into the star-shaped nozzle, if the pressure drop Δp_{byp} is higher than the capillary pressure Δp_{cap} of the liquid in the nozzle center, Fig. 1b. This leads to the following condition for the liquid to enter into the star-shaped nozzle:

$$\Delta p_{\mathrm{byp}} > \Delta p_{\mathrm{cap}} \tag{2}$$

$$\Delta p_{\mathrm{byp}} > \frac{4}{D_{\mathrm{noz}}} \cdot \sigma |\cos \Theta| \tag{3}$$

where D_{noz} stands for the inner diameter of the nozzle, σ describes the surface tension of the liquid, and Θ describes the contact angle of the liquid toward the nozzle material.

For instance, when a constant actuation pressure of 160 hPa (also used in experiments) is applied on the common gas inlet, it leads to a pressure drop along the bypass channels, $\Delta p_{\mathrm{byp}} \approx 100$ hPa (sketch of Fig. 1a), calculated by the standard single-phase finite volume CFD simulations. For simulations, the bypass channels and the

nozzle geometry are meshed with 15 cuboidal cells per 100 μm, and the influence of liquid entering the nozzle is accounted for by obstacles of the approximate droplet size. The obstacles are modeled by a solid phase, as further detailed in the user manual of CFD-ACE + (ESI-Group 2006).

The capillary pressure of the liquid that enters the nozzle can be calculated according to the right hand side of Eq. 3 $\Delta p_{\mathrm{cap}} \approx 75$ hPa. When no liquid is present in the nozzle, Eq. 3 is fulfilled and the liquid enters the nozzle. A liquid plug forms and becomes confined in the center of the nozzle by capillary forces. The gas flow in the bypass channels can still persist, and the gas continuously flows through the nozzle grooves of the star-shaped profile. In response to the liquid column entering the center of the nozzle, on one hand, the pressure drop along the nozzle increases and on the other hand—analog to a resistive voltage divider—the pressure drop Δp_{byp} along the bypass channels decreases. As liquid is present in the nozzle, the simulation calculates a decrease of Δp_{byp} from 100 to 30 hPa, leading to a static pressure increase at the star-shaped nozzle entrance ($L_{\mathrm{noz,in}}$) from 60 to 130 hPa. Assuming a capillary pressure of $\Delta p_{\mathrm{cap}} = 2\sigma \cos\Theta \cdot D_{\mathrm{noz}}^{-1}$ across the interface of a liquid column confined in the center of the nozzle, the pressure inside the liquid column results in 179 hPa. Thus, the pressure in the liquid column at the nozzle entrance is higher than the applied actuation pressure (160 hPa) on the top of the liquid, causing the liquid to retreat. The gas shear flow pulls the liquid plug toward the nozzle outlet, the liquid column becomes constricted, and the droplet finally breaks-off. Hence, the combination of shear induced drag, rising pressure at $L_{\mathrm{noz,in}}$, and capillary forces lead to the droplet break-off. Supported by the gas flow, the droplet is finally transported out of the nozzle as illustrated in Fig. 1c. As long as the droplet is transported toward the outlet, no liquid can re-enter the inlet of the nozzle, due to a high pressure in the region of the converging point of the bypass channels. That is, the pressure drop Δp_{byp} is smaller than the capillary pressure of the liquid in this situation, which prevents the liquid plug from entering the nozzle. Thus, the system provides self-controlled single droplet break-off. After ejection of one droplet, the described sequence restarts as long as the driving actuation pressure is maintained.

3 Fabrication

3.1 MEMS fabrication of the star-shaped nozzle

The essential part of the StarJet dispenser is a star-shaped nozzle which is depicted in Fig. 3. The star-shaped channel profile was first studied as geometry for minimizing the gas bubble resistance in tubes (Metz et al. 2008). For dispensing of liquid metals, the nozzle is fabricated of silicon to provide thermal stability and a high contact angle ($\Theta \geq 150°C$) toward the liquid metal. The nozzle chips are fabricated by bulk micromachining of silicon as follows: The star-shaped nozzle profile and the bypass channels have been etched into a silicon wafer with a thickness of 525 μm first. Therefore, a thermal oxide layer of 1000 nm and a photoresist (Microchemicals AZ 1518) were deposited with a thickness of 2 μm on the top of a silicon wafer, Fig. 5a. The photoresist was structured with the geometry of the bypass channels using an UV light blocking chrome mask, Fig. 5b. After development of the photoresist the oxide layer was structured by means of Reactive Ion Etching (RIE), Fig. 5c. The oxide layer, Fig. 5d, was then coated by a resist film (Microchemicals AZ 9260, 12 μm thickness) that was structured with the star shape, Fig. 5e. The star-shaped nozzle profile was then etched by Deep Reactive Ion Etching (DRIE) into the wafer, up to a residual thickness of 80 μm, Fig. 5f. After stripping the leftover photoresist, the rest of the nozzle and the bypass channels were etched using the oxide layer, which acted as a mask, Fig. 5g. Finally, the wafer was stripped, cleaned and the whole wafer was diced to separate the chips. The complete chip design additionally contains etched pin holes that are employed to align the chips within the actuator.

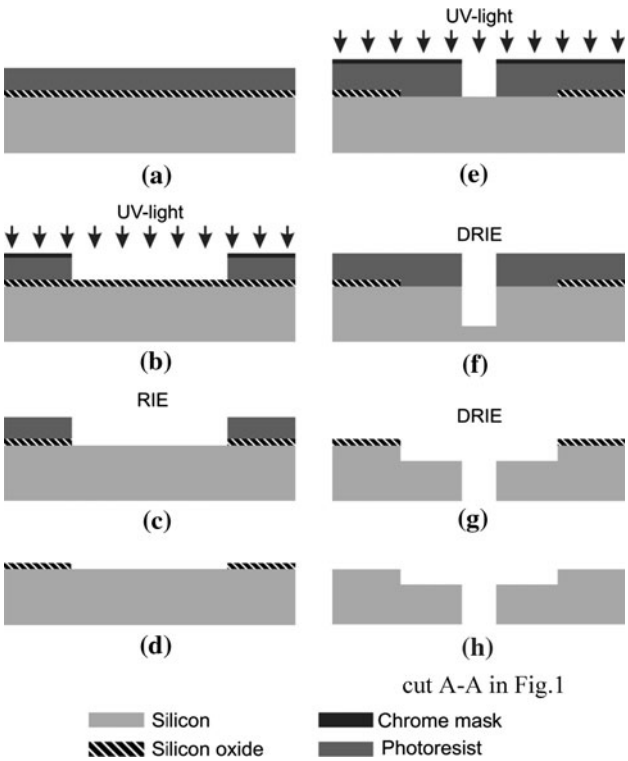

Fig. 5 Fabrication process of the silicon nozzle chip. Subpicture **h** refers to the cut *A–A* in Fig. 3

Table 1 Geometry parameters of the studied StarJet-nozzles

	SJet1	SJet2	SJet3	Units
N	12	12	12	
w_{ch}	40	20	65	μm
d_{ch}	100	100	100	μm
d_{grv}	50	35	70	μm
D_{noz}	183	94	230	μm
p_{cap}	98	192	78	hPa

Figure 3 shows SEM pictures of a StarJet-nozzle chip (SJet4) fabricated by DRIE in its top and angular view. The top view shows the inlet of the nozzle and the bypass channels converging in the center of the nozzle, and lead into the nozzle grooves. The bypass channels transport the gas and the star-shaped profile enables centering of a droplet or plug of the liquid metal in the nozzle due to capillary forces as explained below in more detail.

Three different designs (SJet1, SJet2, SJet3) with parameters as defined in Fig. 3 and Table 1 were fabricated for experimental studies. The nozzle is defined by its inner diameter, the depth of the nozzle grooves, and the number and dimension of the bypass channels. The chip design named SJet1 has twice the inner diameter D_{noz} than the one named SJet2. The value p_{cap} is calculated according to Eq. 3.

3.2 Fabrication of the actuator

The actuator is made from brass due to its favorable properties with respect to mechanical milling and its good thermal conductivity ($\lambda = 120$ W m^{-1} K^{-1}) (Lide 2009). The actuator establishes a fluidic connection to the StarJet-nozzle chips and was designed according to Fig. 2. The actuator features a reservoir for molten metal, a pneumatic connection for the gas supply, an electronically controlled heater, and two access holes for thermocouples to control the temperature of the metal reservoir. The nozzle chips are mechanically clamped to the bottom of the actuator. A drilled hole in the center of the actuator (∅ 400 μm) connects the reservoir to the liquid inlet of the chip. The alignment of the central hole is not critical, as the same condition that prevents the liquid metal from moving into the nozzle grooves of the star-shaped profile protects the bypass channels of the chip from being filled by the liquid metal.

4 Measurements

The experimental results presented in the following demonstrate the performance of the StarJet dispensing method. The StarJet dispenser mainly features two dispensing modes—continuous and DoD mode—of which the continuous mode has been investigated in detail for the SJet1 nozzle.

Figure 6a demonstrates the minimum actuation pressure of 120 hPa for the SJet1 chip. At the described conditions, droplet tear-off has been observed by stroboscopic imaging as shown in Fig. 7a. Below this pressure, no liquid metal is ejected from the orifice, but only a stream of nitrogen gas occurs through the bypass channels. For further testing, the StarJet-prototype as shown in Fig. 5 was actuated with a pressure of 140 and 200 hPa, respectively, while a microphone situated in the gas supply tube recorded pressure waves caused by the dispensing process. Figure 6b, c show periodic and regular waveforms at two different frequencies for the two studied pressure levels. It has to be pointed out that, these pressure oscillations occur spontaneously at specific "natural frequency" as a result of the fluid dynamics inside the dispenser, while the pressure level of the gas supply is maintained at a constant level.

By increasing the actuation pressure incrementally, a linear dependency of the droplet tear-off frequency was observed. Figure 6a depicts the lowest tear-off frequency of about 25 Hz at 120 hPa, the highest of about 120 Hz at 220 hPa with a mainly linear dependency of tear-off frequency on the actuation pressure. While the natural frequency is pressure dependent, the diameter of the dispensed solder droplets is mostly unaffected by the driving pressure level. For different driving pressures in the range of 120–200 hPa, droplet diameters of 210 ± 16 μm have been measured as shown in Figs. 6a and 7b, c. In the actuation pressure range of 140 hPa up to 220 hPa the droplet diameters remain nearly constant with a deviation of only ±6%, Fig. 6a. Further increase of the actuation pressure showed stable tear-off frequencies of up to 300 hPa in the continuous mode. An actuation pressure higher than 300 hPa resulted in a constant liquid jet with subsequent Rayleigh breakup. Another chip design, the SJet2 chip as described in Table 1 is discussed by Metz et al. (2009).

Droplet flight velocities are analyzed, after the droplet left the nozzle outlet by stroboscopic records with a shutter time of 10^{-4} s. These relatively long shutter times result in a motion blur, that is produced from a moving droplet. From the length of the motion blur and the shutter time of the stroboscopic camera, velocities of 2.7 m s^{-1} (at 120 hPa actuation pressure) up to 3.4 m s^{-1} (at 220 hPa) are determined. Thus, the StarJet dispenser provides tunable droplet velocities from nearly 2.5 to 3.5 m s^{-1}, depending on the adjusted actuation pressure level. Wehl et al. (2003) reported velocities during the droplet flight of 4 m s^{-1}, whereas, Schuhmacher et al. (2007) reported tunable droplet velocities ranging from 1 to 2 m s^{-1}. Cao

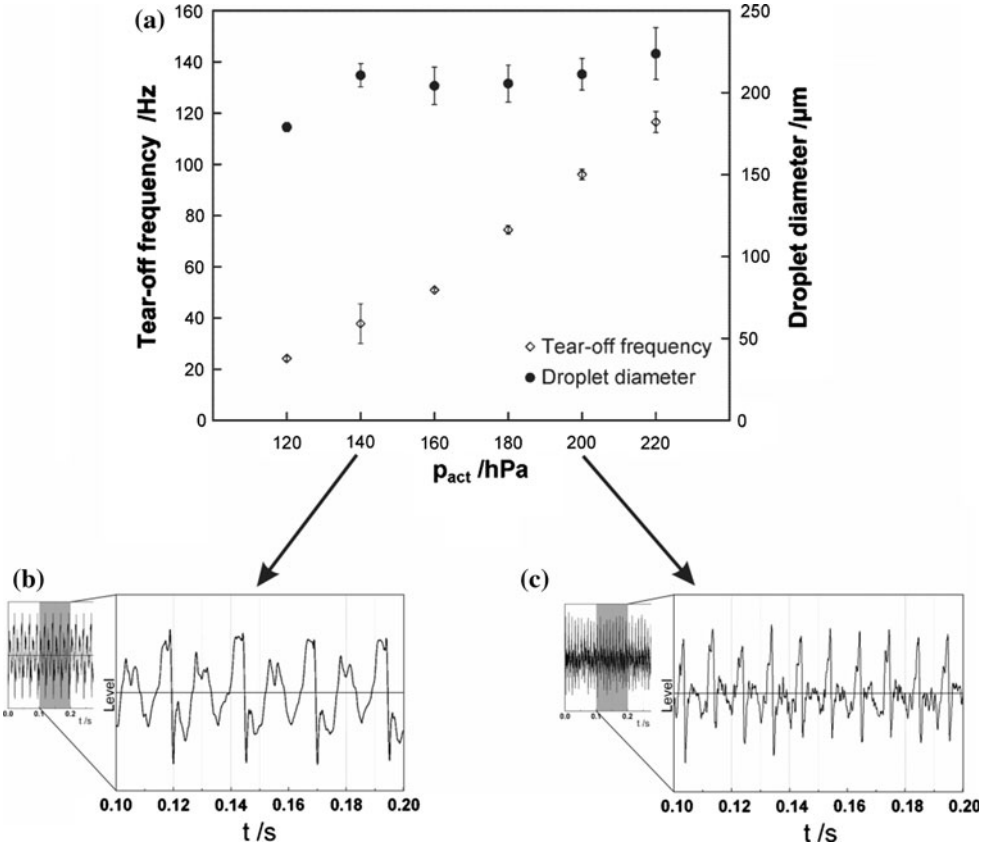

Fig. 6 **a** Droplet tear-off frequencies and droplet diameters as a function of the actuation pressure. **b** Acoustic signal of droplet break-off at actuation pressure of 140 hPa. **c** Acoustic signal of droplet break-off at actuation pressure of 200 hPa

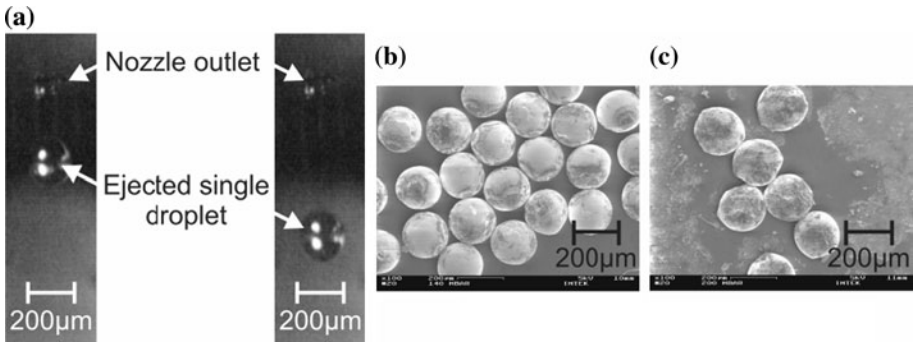

Fig. 7 **a** Solder spheres dispensed at 120 hPa recorded by stroboscopic imaging in flight. **b** SEM pictures of solder spheres dispensed at 140 hPa. **c** SEM pictures of solder spheres dispensed at 200 hPa

et al. (2006) reported drop velocities of 1–8.1 m s^{-1} for their aluminum printer.

To achieve a DoD dispensing mode, a solenoid valve was integrated into the gas supply path. With this valve, the actuation pressure level could be switched on for 6 ms. This pressure impulse is long enough to eject a single solder droplet, but short enough to prevent the formation of a second droplet. With a resting time of up to 20 ms, where the system was rinsed at a lower pressure (50 hPa), it was possible to generate droplets on demand with a frequency up to 38 Hz. Experiments in the DoD dispensing mode are performed with the SJet3 nozzle ($D_{noz} = 230$ µm), and result in droplet sizes of 270 µm with a coefficient of variation of ±16%. In contrast to the DoD mode, the continuous mode produces droplets that match the sizes of the DoD mode, and are measured to be 270 µm ±15%. This result suggests that, the droplet break-off process in DoD mode works the same way as in the continuous mode, except that, the driving pressure is switched off before more than one droplet is ejected.

5 Discussion

A key feature of the StarJet dispenser is that, the star-shaped profile reduces wall friction of droplets as described in detail by Metz et al. (2008). The reduced friction supports the transport decisively and might also reduce

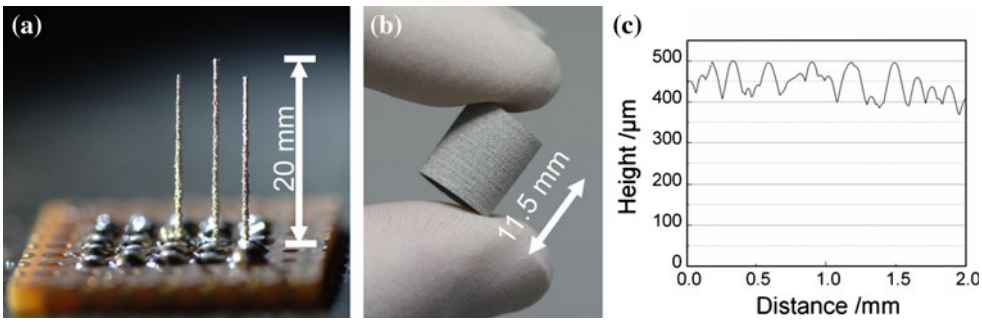

Fig. 8 **a** Three solder columns printed with the StarJet system (IMTEK/Bernd Müller 2010). **b** Printed solder cylinder between fingers. **c** Roughness measurement on the surface of the printed solder cylinder

deflecting forces during ejection. The driving sheath flow reduces oxidation of the hot metal during droplet generation, free flight, and inside the reservoir, if an inert gas such as nitrogen is used. It can be assumed that the sheath flow also contributes to the directional stability of the droplet's flight path by surrounding the droplet in a rotational symmetric manner until it reaches the target.

It follows from the results provided in this article, and the theoretical assessment of the star-shaped channels published previously (Metz et al. 2008) that, the StarJet dispensing method in principle should be well suited for RP applications. First of all, since the droplet diameter is easily adjustable by design in a wide range, printheads with smaller and larger droplets can be used in parallel, to efficiently create larger and smaller features simultaneously. Another key feature in this context is the good reproducibility of droplet diameters of better CV $< 6\%$ for the SJet1 nozzle, which is mandatory for good prototyping results. Furthermore, the high droplet supply frequency in the continuous mode enables large droplet deposition rates, e.g., for printing lines or bulk areas in a continuous movement, while the DoD mode enables controlled deposition in a stepping movement. Finally, practical aspects like the simple set-up and the integrated oxidation protection by the inert nitrogen gas are advantageous for RP applications. For example, during experiments in a typical laboratory environment lasting for 5 h without interruption, no negative effect of oxidation was observed. The ultimate advantage of the presented method is, however, its potential to be realized at higher temperatures and to be employed to other printing materials. Though the present study is confined to a low melting point solder that could also be dispensed with other methods, the simple mechanical setup of the actuator and the high temperature stability of the silicon nozzles suggests that, metals with a higher melting point such as aluminum or silver could be dispensed with the StarJet method also. The challenges associated with higher temperatures, such as, increased thermal stress during cooling down of the dispenser, and higher oxidation rates, as well as practical issues such as eutectic alloy formation between the silicon and the metals to be printed will be subject for future research.

If a good consistency of droplet size is given, the most critical parameter for RP applications is the directional stability of the droplets. Any deviation in the flight path will immediately result in a reduced precision of the fabricated parts. Therefore, the directional stability of droplets produced by the StarJet method has been investigated by simple RP experiments. The focus of these experiments was not to create sophisticated 3D structures, but to explore the limits of resolution and precision achievable by simple means. Therefore, simple 3D structures were printed onto an aluminum substrate in the DoD and in the continuous mode. The distance between the dispenser and the substrate was kept constant at 15 mm during this test. Of course, printing from such large distance does not result in optimum performance for prototyping, but is assistive to determine the directional stability of the droplets. As shown in Fig. 8a, DoD printing of solder columns with a height up to 30 mm with a column width between 500 µm and 1 mm was possible, resulting in aspect ratios of 30–60, which corresponds well to results of Lee et al. (2008), who report aspect ratios of 22 in their study. Figure 8b depicts, printed cylindrical structures that have been created in the continuous dispensing mode by a constant rotating motion of the substrate table. For these structures, aspect ratios of 35–40 and a wall thickness of 315 µm have been determined. The measurement of the surface roughness depicted in Fig. 8c shows that the roughness is about 100 µm.

6 Conclusion

The StarJet method studied in this study, provides a new concept for printing micro droplets of liquid metal by a simple pneumatic actuation mechanism. The self-regulated droplet tear-off principle is based on capillary fluid dynamics occurring within the star-shaped nozzle manufactured by means of bulk micromachining of silicon. The first prototype of the StarJet dispenser was characterized with respect to RP applications using a nozzle of type SJet1 and SJet3.

Two main different working modes of the StarJet device have been demonstrated: a continuous droplet generation

and a drop on demand (DoD) mode. A nearly mono-dispersed particle distribution, largely independent of actuation pressure, was achieved in both modes. In the continuous mode, a linear dependency of the droplet tear-off frequency (25–120 Hz), on the driving actuation pressure (120–220 hPa) could be observed, whereas, the droplet diameters were measured as 210 ± 16 µm using a nozzle with an inner diameter of 183 µm. Hence, by adjustment of the actuation pressure, the dispensing frequency could be controlled, but droplet diameters remained nearly constant. This characteristic of the StarJet dispenser implies great importance for RP of microstructures.

Nozzle designs with different dimensions studied by experiments in this study and in previous publications by Metz et al. (2009), demonstrates that, this method is in principle scalable to deliver droplets of various sizes in the pl- to nl-range. An inherent advantage of the method is that, the actuating gas flow protects the molten metal from oxidation and probably contributes to the good directional stability of the printed droplets. The resulting aspect ratio of printed structures of 30 and higher, proves the excellent directional stability and underlines the suitability of this technology for RP. However, more research is required to fully describe the droplet generation mechanism, and to be able to predict droplet size and natural frequency of the continuous dispensing mode. In addition, the alternative application fields might request a transfer of the StarJet method to dispensing of the rheological complex fluids, as well as to aqueous solutions, which in turn requires technologies to adjust the contact angle on the nozzle material appropriately. The high temperature stability of the dispenser, which is not limited by the Curie temperature, as it is in the case for piezoelectric driven devices, allows for further investigations using metals with higher melting points as printing material.

7 Experimental section

The function of the StarJet dispenser requires a high contact angle of molten metal of about $\Theta = 150°$ on the nozzle material (cf. Fig. 2). In order to determine the contact angle on silicon oxide that is effective in the star-shaped nozzle, contact angle measurements have been performed. Therefore, an oxidized silicon wafer was heated up to 250°C in a nitrogen environment. The nitrogen environment was established using a gas tight box, into which the heater, as well as the heated silicon wafer, were placed. The box was rinsed by nitrogen gas during both, the deposition of the solder droplets on the heated silicon oxide substrate and during cool-down. After the solder and the substrate cooled down, contact angle measurements with the Dataphysics OCA15plus system were performed. As a result, the advancing contact angle was determined as $\Theta = 156° \pm 3°$. This value justifies the design of the star-shaped nozzles as presented in Table 1.

Due to the necessity of high contact angles of the molten solder toward silicon, flux free solder has been selected as material. For the experiments, only the solder type $Sn_{95}Ag_4Cu_1$ (melting temperature $T_{liq} = 213°C$) (Stannol GmbH MSDS 2010) was used. The density of the molten solder is $\rho = 7500$ kg m^{-3} (Stannol GmbH MSDS 2010). The value of surface tension of the solder type $Sn_{95}Ag_4Cu_1$ is unknown, but it was assumed to be nearly equal to a similar solder type $Sn_{96.5}Ag_{3.5}$ for which a surface tension of $\sigma = 493$ mN m^{-1} is known (Glazer 1994).

The actuator to drive the silicon chips is described in detail in the results section. In addition to the actuator, the periphery of the StarJet system consists of an external fast switching 3/2-way solenoid valve (MAC® Valves 34B-ABA-GDFC-1BA) for switching the sheath gas nitrogen flow between two pressure levels for the supply of the actuator. The solenoid valve switches between an adjustable low pressure level (50 hPa) for constant rinsing with sheath gas, and an adjustable higher pressure level to actuate the system. The control unit which drives the solenoid valve is controlled by a PC. Two pressure control valves, two manometers, each for one pressure level, connection tubes, and a pressure reservoir constitute the fluidic periphery of the StarJet system. The actuator is heated by a cartridge heater with a power of 80 W. The temperature is controlled during the experiments with a thermocouple near the chip. The temperature was controlled to 220 ± 3°C. For the observation of droplets, the setup was placed in front of a stroboscopic camera. A microphone capsule, which was integrated in the fluidic path of the gas in the pneumatic supply tubing, was used to determine pressure disturbances during droplet break-off. The analysis of the audio signal and the extraction of the natural frequency were done by the software Audacity.

The measurement of the solder sphere diameters was carried out with a Zeiss AxioObserver Z1 system and its automated detection software AxioVision Rel. 4.8. The nearly spherical geometry of the droplets was confirmed by dispensing the molten droplets into a soap/water mixture. Due to the low surface tension and the low temperature (approx. 20°C) of the soap/water mixture, negligible deformation and fast solidification of the molten droplets were assured. An amount of 20 spheres in one photograph has been measured at a time.

Acknowledgments The authors gratefully acknowledge the financial support from the Deutsche Forschungsgemeinschaft for the project ZI/1201/3-1 in the priority program SPP 1423.

References

Agarwala M, Bourell D, Beaman J, Marcus H, Barlow J (1995) Direct selective laser sintering of metals. Rapid Prototyp J 1:26–36

Attinger D, Haferl S, Zhao Z, Poulikakos D (2000) Transport phenomena in the impact of a Molten droplet on a surface: macroscopic phenomenology and microscopic considerations. Part II heat transfer and solidification. Annu Rev Heat Transf 11:145–205

Cao W, Miyamoto Y (2006) Freeform fabrication of aluminum parts by direct deposition of molten aluminum. J Mater Process Technol 173:209–212

De Heij B, Daub M, Gutmann O, Niekrawietz R, Sandmaier H, Zengerle R (2004) Formation of dispersions using "flow focusing" in microchannels. Anal Bioanal Chem 378:119–122

ESI-Group, Software (2006) CFD-ACE + 2007

Essien M, Keicher DM, Miller WD (2000) Manufacturing electronics components in a direct-write process using precision spraying and laser irradiation. Optomec Design Company, CA Patent 2,373,149 A1

Glazer J (1994) Microstructure and mechanical-properties of Pb-free solder alloys for low-cost electronic assembly—a review. J Electron Mater 23:693–700

Haferl S, Poulikakos D (2002) Transport and solidification phenomena in molten microdroplet pileup. J Appl Phys 92:1675–1689

Haferl S, Attinger D, Zhao Z, Giannakouros J, Poulikakos D (2000) Transport phenomena in the impact of a molten droplet on a surface: macroscopic phenomenology and microscopic considerations. Part I fluid dynamics. Annu Rev Heat Transf 11:65–143

Hayes DJ, Wallace DB, Cox WR (1999) MicroJet printing of solder and polymers for multi-chip modules and chip-scale packages. In: Proceedings of international microelectronics and packaging conference & exhibition

Heinzl J, Hertz CH (1985) Ink-Jet printing. Adv Image Elec Phys 65:91–171

Irlinger F, Harnisch J (2005) Hochtemperatur-Tropfenerzeugung mittels eines elektromagnetischen drop-on-demand-systems. In: Proceedings of Mikrosystemtechnik Kongress, pp 325–328

Larson R (1998) Arcam Limited. U.S. Patent 5,786,562

Lee T-M, Kang TG, Yang J-S, Jo J, Kim K-Y, Choi B-O (2008) Drop-on-demand solder droplet jetting system for fabricating microstructure. IEEE Trans Electron Packag Manuf 31:202–210

Lide DR (ed) (2009) Thermal conductivity of alloys as a function of temperature. In: CRC handbook chemistry and physics, 89th edn. CRC Press/Taylor and Francis, Boca Raton, FL

Madou MJ (2002) Fundamentals of microfabrication: the science of miniaturization, 2nd edn. CRC Press, Boca Raton, FL

Megaridis CM, Boomsma K, Bayer IS (2004) Partial rebound of molten-metal droplets impacting on solid substrates. AIChE J 50:1356–1363

Metz T, Streule W, Zengerle R, Koltay P (2008) StarTube: a tube with reduced contact line for minimized gas bubble resistance. Langmuir 24:9204–9206

Metz T, Birkle G, Zengerle R, Koltay P (2009) StarJet: pneumatic dispensing of nano- to picoliter droplets of liquid metal. In: Proceedings of 22nd IEEE international conference on MEMS, pp 43–46

Orme M, Willis K, Nguyen T-V (1993) Droplet patterns from capillary stream breakup. Phys Fluids A 5:80–90

Rayleigh L (1878) On the instability of jets. Proc Lond Math Soc 10:4–13

Sachs EM, Haggerty JS, Cima MJ, Williams PA (1993) Three-dimensional printing techniques. Massachusetts Institute of Technology, U.S. Patent 5,204,055. http://open3dp.me.washington.edu/wp-content/uploads/2009/11/3DP_techniques_52040551.pdf

Schuhmacher D, Niekrawietz R, Scheithauer H, De Heij B, Alavi M, Zengerle R, Koltay P (2007) Production of solder microdroplets using a highly parallel and contact-free printing method. In: Proceedings of 19th international conference on micro electro mechanical systems, pp 357–360

Sedlacek V (1986) Non-ferrous metals and alloys. Elsevier Science Ltd, Amsterdam

Stannol GmbH, Material safety data sheet for $Sn_{95}Ag_4Cu_1$ (2010)

Tsung Pan AI, Ross RA, Hanson EG (1998) Solder jet printhead. Hewlett-Packard Company, U.S. Patent 5,779,971

Waldvogel JM, Poulikakos D, Wallace DB, Marusak R (1996) Transport phenomena in picoliter size solder droplet dispension. J Heat Transf-Trans Asme 118:148–156

Wang XH, Fuh JYH, Wong YS, Lu L, Loh HT, Tang YX, Zhu HH (2003) Formation of copper-based metal part via direct laser sintering. Mater Sci Forum 437–438:273–276

Wehl W, Wild J, Lemmermeyer B (2003) A drop-on-demand metal jet printer for wafer bumping. In: Proceedings of 14th international microelectronics and packaging conference & exhibition

Wehl W, Kuebler M, Lemmermeyer B, Wild J (2006) Ein akustisches antriebssystem fuer einen Drop-on-Demand-Druckkopf. Horizonte 28:3–9

Wu G, Langrana NA, Sadanji R, Danforth S (2001) Solid freeform fabrication of metal components using fused deposition of metals. Mater Eng 23:97–105

Yamaguchi K, Nakamoto T, Abraha P (1995) Consideration on the optimum conditions to produce micromechanical parts by photo polymerization using direct focused beam writing. In: Proceedings of 6th international symposium on micro machine and human science, pp 71–76